



## Collective excitations of $\Lambda$ hypernuclei

K. Hagino<sup>a</sup>, J.M. Yao<sup>b</sup>, F. Minato<sup>c</sup>, Z.P. Li<sup>b</sup>, M. Thi Win<sup>a</sup>

<sup>a</sup>Department of Physics, Tohoku University, Sendai 980-8578, Japan

<sup>b</sup>School of Physical Science and Technology, Southwest University, Chongqing 400715, China

<sup>c</sup>Research Group for Applied Nuclear Physics, Japan Atomic Energy Agency, Tokai 319-1195, Japan

---

### Abstract

We discuss low-lying collective excitations of  $\Lambda$  hypernuclei using the self-consistent mean-field approaches. We first discuss the deformation properties of  $\Lambda$  hypernuclei in the  $sd$ -shell region. Based on the relativistic mean-field (RMF) approach, we show that the oblate deformation for  $^{28}\text{Si}$  may disappear when a  $\Lambda$  particle is added to this nucleus. We then discuss the rotational excitations of  $^{25}_{\Lambda}\text{Mg}$  using the three-dimensional potential energy surface in the deformation plane obtained with the Skyrme-Hartree-Fock method. The deformation of  $^{25}_{\Lambda}\text{Mg}$  is predicted to be slightly reduced due to an addition of a  $\Lambda$  particle. We demonstrate that this leads to a reduction of electromagnetic transition probability,  $B(E2)$ , in the ground state rotational band. We also present an application of random phase approximation (RPA) to hypernuclei, and show that a new dipole mode, which we call a soft dipole  $\Lambda$  mode, appears in hypernuclei, which can be interpreted as an oscillation of the  $\Lambda$  particle against the core nucleus.

© 2012 Published by Elsevier Ltd.

**Keywords:** impurity effect, deformation, rotational excitation, dipole motion, mean-field models, random phase approximation

---

### 1. Introduction

One of the main interests in hypernuclear physics is to investigate how an addition of a  $\Lambda$  particle influences the structure of atomic nuclei. A characteristic feature of the  $\Lambda$  particle is that it is free from the Pauli principle for nucleons, and thus it can deeply penetrate into the nuclear interior. A  $\Lambda$  particle may modify several properties of nuclei, such as nuclear size[1, 2], the density distribution[3], deformation properties [4, 5, 6, 7, 8, 9, 10, 11], the neutron drip-line[12, 13], and fission barrier[14].

In this contribution, we discuss the impurity effect of a  $\Lambda$  particle on collective excitations. It is well known that low-lying states in even-even nuclei show a collective character, strongly reflecting the shell structure and pairing correlation. These collective excitations are one of the most important aspects of many-body systems, and have been extensively studied in the past. Two types of collective motion are well known: a rotational motion of deformed nuclei and a vibrational motion of spherical nuclei. In this paper, we particularly investigate the ground state rotational band of a deformed hypernucleus as well as the low-lying dipole motion of a spherical hypernucleus.

In the next section, we first discuss the deformation properties of hypernuclei in the  $sd$ -shell region. In Section 3, we investigate the rotational motion of a deformed hypernucleus,  $^{25}_{\Lambda}\text{Mg}$ . To this end, we employ the collective Hamiltonian approach based on the density functional theory. In Section 4, we discuss vibrational excitations of a spherical hypernucleus,  $^{18}_{\Lambda\Lambda}\text{O}$ . We particularly study the dipole motion, and show that a new dipole mode appears in hypernuclei, which is absent in ordinary nuclei. We then summarize the paper in Section 5.

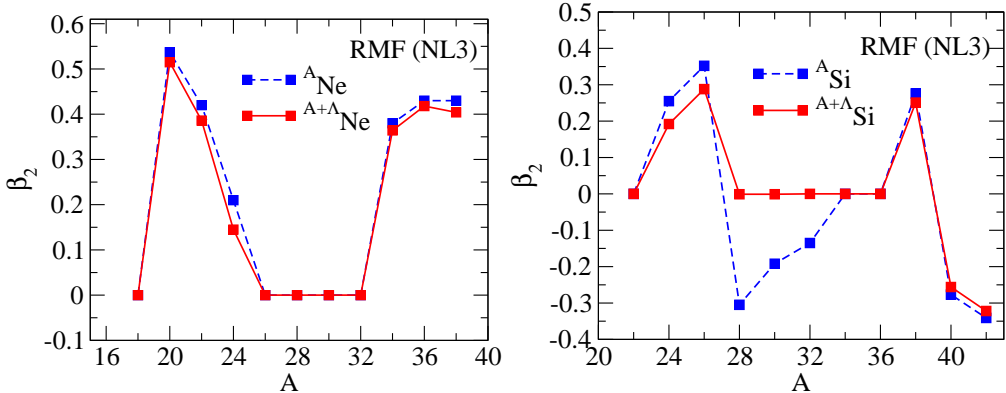


Figure 1. Quadrupole deformation parameter  $\beta_2$  for Ne (left panel) and Si (right panel) isotopes obtained with the RMF method with the NL3 parameter set. The dashed lines show the deformation parameter for the core nucleus, while the solid lines for the corresponding hypernucleus.

## 2. Deformation of hypernuclei

It is well known that many open-shell nuclei are deformed in the ground state. A clear evidence for nuclear deformation is provided by a rotational spectrum, which scales as  $E_I \propto I(I+1)$  as a function of the angular momentum  $I$ . In order to investigate how the nuclear deformation is affected by a  $\Lambda$  particle, we employ the self-consistent mean-field theory [15]. With this method, the optimum density distribution is obtained automatically by minimizing the total energy, and thus it is well suited for a discussion of polarization effects due to a  $\Lambda$  particle.

It is probably Žofka who applied the self-consistent method to deformed hypernuclei for the first time [4]. He used Gaussian interactions for nucleon-nucleon ( $NN$ ) and nucleon-Lambda ( $N\Lambda$ ) interactions and showed that a  $\Lambda$  particle changes the quadrupole moment, which is proportional to the deformation parameter, at most by 5 % in the  $sd$ -shell region. This result is consistent with the results of more recent Skyrme-Hartree-Fock (SHF) calculations for axially deformed hypernuclei[5].

We carry out a similar study using the relativistic mean field (RMF) method as an alternative choice of effective  $NN$  and  $N\Lambda$  interactions [6]. In the RMF approach, nucleons and a  $\Lambda$  particle are treated as structureless Dirac particles interacting through the exchange of virtual mesons, that is, the isoscalar scalar  $\sigma$  meson, the isoscalar vector  $\omega$  meson, and the isovector vector  $\rho$  meson[12, 16] (see also Ref. [17] for the zero range approximation to RMF, that is, the relativistic point coupling model for hypernuclei). The photon field is also taken into account to describe the Coulomb interaction between protons.

Figure 1 shows the deformation parameter for the ground state of Ne and Si isotopes obtained with the NL3 parameter set of RMF [18]. We have assumed axial symmetry for the density distribution, and put a  $\Lambda$  particle in the lowest single-particle orbit. The pairing correlation among the nucleons is also taken into account in the constant gap approximation. The dashed lines show the deformation parameter for the even-even core nuclei, while the solid lines are for the corresponding hypernuclei. We see that the change in the deformation parameter for most of the nuclei shown in the figure is small, being consistent with the previous non-relativistic self-consistent calculations [4, 5]. However, we find a few important exceptions. Those are the  $^{28,30,32}\text{Si}$  nuclei, for which the deformation parameter vanishes when a  $\Lambda$  particle is added.

In order to understand the origin for the disappearance of nuclear deformation, Fig. 2 shows the potential energy surfaces for the  $^{23}_{\Lambda}\text{Ne}$  and  $^{29}_{\Lambda}\text{Si}$  nuclei. The energy surfaces for the corresponding core nuclei are also shown. In order to facilitate the comparison, we shift the energy surface for the hypernuclei by a constant amount as indicated in the figures. In contrast to the  $^{22}\text{Ne}$  nucleus, which has a deep prolate minimum in the energy surface, the energy surface for the  $^{28}\text{Si}$  nucleus shows a relatively shallow oblate minimum, with a shoulder at the spherical configuration. The energy difference between the oblate and the spherical configurations is 0.754 MeV, and could be easily inverted when a  $\Lambda$  particle is added.

The disappearance of nuclear deformation was not observed in the previous SHF calculations [5]. In Ref. [7], we have compared the SHF and RMF approaches and have shown that the different results between the two approaches

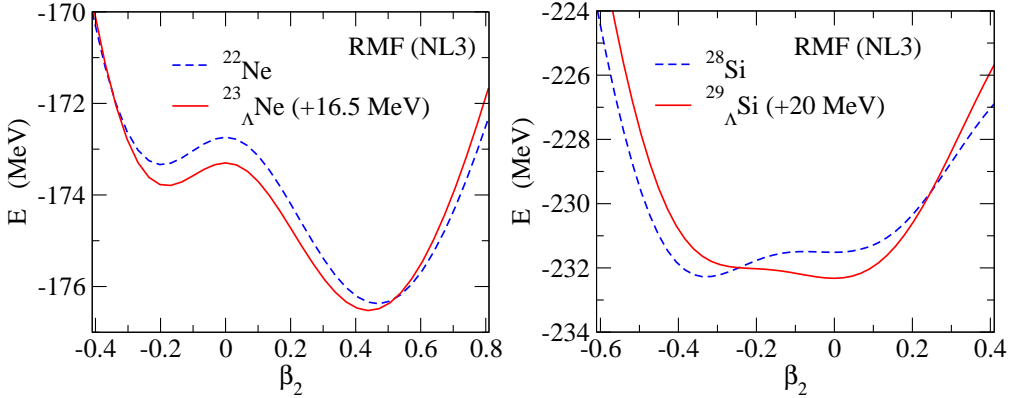


Figure 2. (Left panel) The potential energy surface for  $^{22}\text{Ne}$  (the dashed line) and  $^{23}\Lambda\text{Ne}$  (the solid line) nuclei obtained with the RMF method. The energy surface for  $^{23}\Lambda\text{Ne}$  is shifted by a constant amount as indicated in the figure. (Right panel) The same as the left panel, but for  $^{28}\text{Si}$  and  $^{29}\Lambda\text{Si}$  nuclei.

with respect to nuclear deformation come about because the RMF yields a somewhat stronger polarization effect of the  $\Lambda$  hyperon than that of the SHF approach. We have shown that the deformation disappears also in the SHF approach if the energy difference between the optimum deformation and the spherical configuration is less than about 1 MeV [7].

Our RMF calculations indicate that the oblate deformation of the  $^{12}\text{C}$  nucleus also disappears when a  $\Lambda$  particle is added [6]. It is interesting to notice that the recent anti-symmetrized molecular dynamics (AMD) calculation by Isaka *et al.* also exhibits a similar disappearance of deformation for the  $^{12}\text{C}$  nucleus[11].

### 3. Rotational excitations of deformed hypernuclei

In the previous section, we presented results of RMF calculations, in which the axially symmetric shape of hypernuclei was assumed. Subsequently, three-dimensional (3D) mean-field calculations have also been performed both with SHF [8] and RMF [10], taking into account triaxial deformation,  $\gamma$ . In this section, we discuss the rotational spectra of deformed hypernuclei on the basis of such 3D calculations with SHF.

In order to obtain a spectrum with the density functional theory, one has to go beyond the mean field approximation, in which a many-body wave function is assumed to be given by a single Slater determinant. One standard way to do so is to perform generator-coordinate-method (GCM) calculations, in which many Slater determinants are superposed after angular-momentum and particle-number projections [19, 20, 21, 22]. It is, however, still difficult to apply it to odd-mass nuclei, such as single- $\Lambda$  hypernuclei, which has a half-integer spin and in which the time reversal symmetry is broken. We therefore employ the five dimensional collective Bohr Hamiltonian approach [23, 24]. This is based on the so called Gaussian overlap approximation (GOA) to GCM, in which the overlap between two Slater determinants behaves as a Gaussian function of a generator coordinate.

In this method, the collective Hamiltonian for a quadrupole motions, with the intrinsic (deformation) coordinates of  $\beta$  and  $\gamma$  together with the three-dimensional spatial rotation, is constructed as

$$H_{\text{coll}} = T_{\text{vib}} + \frac{1}{2} \sum_{k=1}^3 \frac{I_k^2}{2\mathcal{J}_k} + V_{\text{coll}}(\beta, \gamma), \quad (1)$$

where  $T_{\text{vib}}$  is the kinetic energy operator for the vibrational motions, while  $V_{\text{coll}}$  is the collective potential. The vibrational moment inertia in  $T_{\text{vib}}$  and the rotational moment of inertia  $\mathcal{J}_k$  in the second term of Eq. (1) are calculated with the cranking approximation using the single-particle wave functions. The collective potential  $V_{\text{coll}}$  is calculated as a sum of the total energy in the mean-field approximation and corrections due to the vibrational and rotational zero point motions.

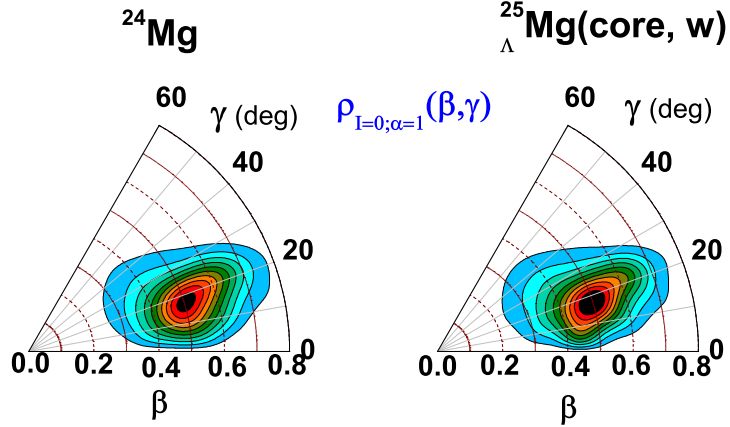


Figure 3. The probability distribution in the  $(\beta, \gamma)$  deformation plane for the ground state of  $^{24}\text{Mg}$  without (the left panel) and with (the right panel) the  $\Lambda$  particle.

Based on the idea of the particle-rotor/vibrator model, the total Hamiltonian for hypernuclei can be divided into the collective part for the nuclear core, the single-particle part for hyperon, and the interaction part between the nuclear core and hyperon[25, 26]. In this article, we focus on how the core nucleus is modified by the addition of a  $\Lambda$  particle[9]. We therefore apply the collective Hamiltonian approach only to the collective part of the Hamiltonian for the nuclear core,

$$H_{\text{coll}}^{(\text{core})} = T_{\text{vib}} + \frac{1}{2} \sum_{k=1}^3 \frac{I_k^2}{2J_k} + V_{\text{coll}}^{(\text{core})}(\beta, \gamma). \quad (2)$$

We mention that there is a small ambiguity here concerning how to define the collective potential for the core nucleus,  $V_{\text{coll}}^{(\text{core})}$ , due to the  $N\Lambda$  interaction in the energy functional. Here we consider two options: in one option, the  $N\Lambda$  interaction is not included in  $V_{\text{coll}}^{(\text{core})}$  at all (this option is labeled as “w/o” below), and in the other the whole of the  $N\Lambda$  interaction is included in  $V_{\text{coll}}^{(\text{core})}$  (labeled as “w”).

By solving the collective Hamiltonian, one can construct the spectrum of a nucleus by taking into account the fluctuation around the minimum of the collective potential. Fig. 3 shows the probability distribution in the  $(\beta, \gamma)$  deformation plane for the ground state of  $^{24}\text{Mg}$  when the  $\Lambda$  particle is absent (the left panel) and present (the right panel). To this end, we use the SGII parameter set [27] for the Skyrme interaction for the  $NN$  interaction and the No. 1 set of Ref. [28] for the  $N\Lambda$  interaction. We take the option “w” for the contribution of the  $N\Lambda$  interaction to the collective potential. One finds that the  $\Lambda$  particle slightly shifts the probability distribution towards the smaller deformation region. The average values for  $\beta$  and  $\gamma$  are 0.54 and  $20.0^\circ$ , respectively, for the  $^{24}\text{Mg}$  nucleus without  $\Lambda$ , which are altered to 0.52 and  $20.8^\circ$  when the  $\Lambda$  particle is added. We find that the change in the proton radius is much smaller, only by around 0.5 % [9]. Therefore, the dominant effect of the  $\Lambda$  particle in this mass region is to make the deformation parameter smaller, rather than to shrink the whole nucleus.

Figure 4 shows the calculated spectra for the ground state rotational band. One can see that the  $\Lambda$  stretches the spectra of ground state band. That is, the  $\Lambda$  particle increases the excitation energy of the  $2_1^+$  state by  $\sim 7\%$ . At the same time, it reduces the  $E2$  transition strength  $B(E2 : 2_1^+ \rightarrow 0_1^+)$  by  $\sim 9\%$ . Notice that since the  $\Lambda$  particle is neutral-charge, the  $E2$  transition strength of the whole hypernucleus is given by the protons in the nuclear core. Therefore, the calculated  $B(E2)$  value of the nuclear core can be compared with the  $B(E2)$  value of the hypernucleus. Recent AMD calculations indeed yield a similar reduction in the  $B(E2)$  value for  $^{25}_{\Lambda}\text{Mg}$ , although they suggest a compression of the rotational spectrum [30]. It will be an interesting future work to investigate how the rotational spectrum is affected when the  $\Lambda$  particle contribution to the total Hamiltonian is taken into account.

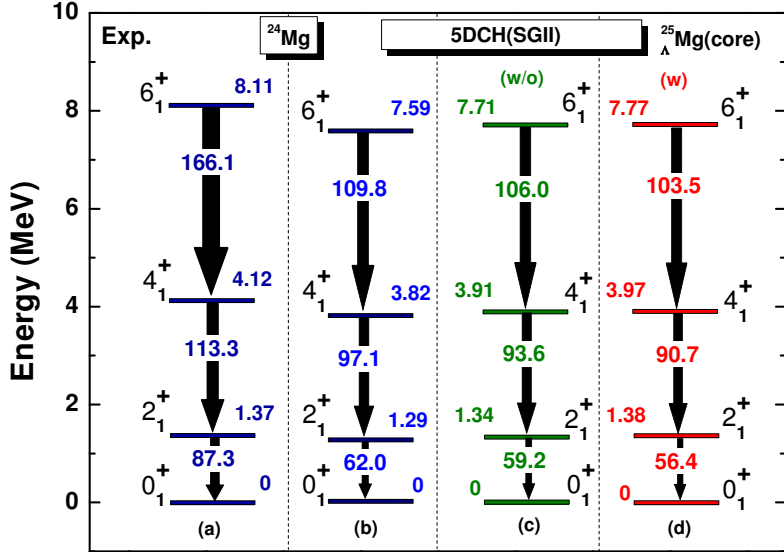


Figure 4. The low-spin spectra of the ground state rotational band for the  $^{24}\text{Mg}$  (b) and the nuclear core of  $^{25}_{\Lambda}\text{Mg}$  (c, d) obtained with the five-dimensional collective Hamiltonian (5DCH). The  $B(E2)$  values are in units of  $e^2 \text{ fm}^4$ . The spectrum of  $^{24}\text{Mg}$  is compared with the corresponding experimental data (a), taken from Ref. [29].

#### 4. Soft dipole motion of spherical hypernuclei

Let us next discuss vibrational excitations of spherical hypernuclei. For vibrational excitations, the random phase approximation (RPA) has provided a convenient and useful method [26, 31]. This method describes a small amplitude oscillation around the Hartree-Fock minimum in the potential energy surface. The excited phonon states are thus given in this method as a superposition of many 1-particle 1-hole states. This method has been successfully applied to many nuclei in order to describe low-lying collective vibrations as well as several types of giant resonances. See, e.g., Ref. [32] for a recent application to the giant dipole resonance in the Nd and Sm isotopes.

One can generalize this scheme to hypernuclei [33]. As in the previous section, an application to single- $\Lambda$  hypernuclei is complicated, and in this article we consider only double- $\Lambda$  hypernuclei, for which the ground state always has a spin and parity of  $0^+$ . Such calculations will provide the upper limit of the impurity effect for single- $\Lambda$  hypernuclei. In RPA, excited states of hypernuclei are built onto the ground state  $|0\rangle$  as  $|k\rangle = Q_k^\dagger |0\rangle$  with

$$Q_k^\dagger = \sum_{p,h \in n,p,\Lambda} (X_{ph}^{(k)} a_p^\dagger a_h - Y_{ph}^{(k)} a_h^\dagger a_p), \quad (3)$$

where  $X_{ph}^{(k)}$  and  $Y_{ph}^{(k)}$  are the forward and backward amplitudes, respectively.  $a_p^\dagger$  and  $a_h^\dagger$  are the creation operators for a particle state  $p$  (*i.e.*, a single-particle state above the Fermi energy) and for a hole state  $h$  (*i.e.*, a single-particle state below the Fermi energy), respectively, for protons, neutrons, and  $\Lambda$  particles. The amplitudes  $X_{ph}^{(k)}$  and  $Y_{ph}^{(k)}$ , as well as the excitation energy  $E_k$  are obtained by solving the RPA equations, which include residual interactions. The electric transition probabilities from the excited state to the ground state are computed as

$$B(E\lambda : k \rightarrow 0) = |\langle k|F|0\rangle|^2, \quad (4)$$

with the excitation operators of

$$F_{\lambda\mu} = e \sum_{i \in p} r_i^\lambda Y_{\lambda\mu}(\hat{\mathbf{r}}_i), \quad (5)$$

nucleus	$2_1^+$ state		$3_1^-$ state	
	$E$ (MeV)	$B(E2)$ ( $e^2 \text{fm}^4$ )	$E$ (MeV)	$B(E3)$ ( $e^2 \text{fm}^6$ )
$^{16}\text{O}$	13.1	0.726	6.06	91.1
$^{18}_{\Lambda\Lambda}\text{O}$	13.8	0.529	6.32	67.7

Table 1. The excitation energies and the electromagnetic transition probabilities,  $B(E2)$  and  $B(E3)$ , for the first  $2^+$  and  $3^-$  states of  $^{16}\text{O}$  and  $^{18}_{\Lambda\Lambda}\text{O}$  nuclei obtained with the Skyrme-HF+RPA method.

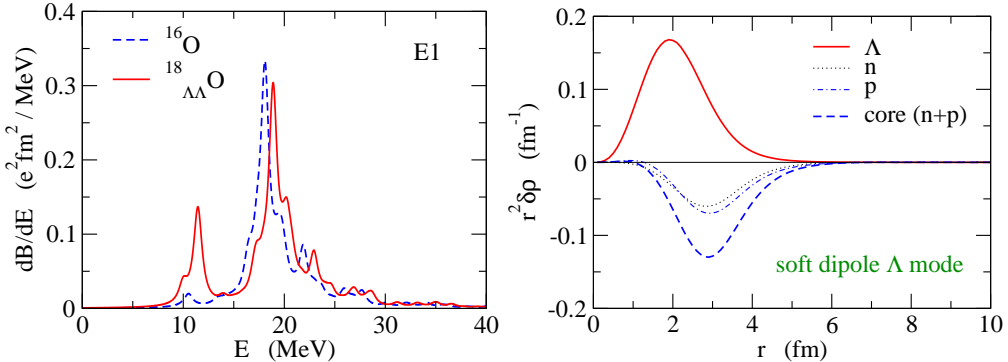


Figure 5. (Left panel) The strength distribution for the electric dipole (E1) excitations of the  $^{16}\text{O}$  nucleus (the dashed line) and the  $^{18}_{\Lambda\Lambda}\text{O}$  nucleus (the solid line). These are obtained by smearing the RPA strength distributions with a Lorenzian function with a width of 1 MeV. (Right panel) The transition density for the soft dipole state at 11.4 MeV in the  $^{18}_{\Lambda\Lambda}\text{O}$  nucleus.

for  $\lambda \geq 2$  and

$$F_{\lambda=1,\mu} = e \sum_{i \in p} (r_i Y_{1\mu}(\hat{\mathbf{r}}_i) - R Y_{1\mu}(\hat{\mathbf{R}})), \quad (6)$$

for  $\lambda = 1$  (that is, the E1 response), where

$$\mathbf{R} = \frac{1}{m_N(Z+N) + m_\Lambda N_\Lambda} \left( m_N \sum_{i \in n,p} \mathbf{r}_i + m_\Lambda \sum_{i \in \Lambda} \mathbf{r}_i \right), \quad (7)$$

is the center of mass of the hypernucleus, and  $m_N$  and  $m_\Lambda$  are the mass of nucleon and  $\Lambda$  hyperon, respectively.  $N$ ,  $Z$  and  $N_\Lambda$  are the number of neutrons, protons and  $\Lambda$  hyperons, respectively.

We apply the RPA method to the  $^{18}_{\Lambda\Lambda}\text{O}$  nucleus. To this end, we use the SkM\* parameter set of the Skyrme interaction for  $NN$  interaction [34], and the No.5 parameter set in Ref.[28] for the  $\Lambda N$  interaction. For the  $\Lambda\Lambda$  interaction, we use the S $\Lambda\Lambda$ 1 parameter set evaluated by Lanskoy[35], although this parameter set may overestimate the  $\Lambda\Lambda$  binding energy. The results for the lowest  $2^+$  and  $3^-$  states are summarized in Table 1. We see that the  $\Lambda$  particles slightly reduce the collectivity both for the quadrupole and octupole modes of excitations. That is, the excitation energies are increased while the electromagnetic transition probabilities are decreased by 26-28%. This is qualitatively similar to the results for the rotational excitation presented in the previous section. In RPA, the increase in the excitation energies can be understood in terms of the change in neutron and proton single-particle energies due to the  $\Lambda$  particles. That is, the  $\Lambda$  particles affects most strongly the energy for deeply bound states, such as  $1s_{1/2}$  state, while the change is smaller for single-particle states close to the Fermi surface[33].

The left panel of Fig. 5 shows the strength distribution for the electric dipole (E1) excitation, weighted by a Lorenzian function with a width of 1.0 MeV. The solid and dashed lines denote the results for the  $^{18}_{\Lambda\Lambda}\text{O}$  and  $^{16}\text{O}$  nuclei, respectively. This figure indicates that the addition of  $\Lambda$  particles shifts the giant dipole resonance (GDR) peak around  $\sim 18$  MeV toward a high energy. This feature is similar to the low-lying states shown in Table 1. We have found that giant resonances with other multipolarities, such as giant monopole resonance (GMR) and giant quadrupole resonance (GQR), show a similar behavior[33].

In addition to the shift of the GDR peak, the dipole strength distribution for  $^{18}_{\Lambda\Lambda}\text{O}$  shows an additional peak at 11.4 MeV. This peak appears only when the  $\Lambda$  hyperons are added to the  $^{16}\text{O}$  nucleus, and a similar peak is not seen in other modes of excitations. The strongest RPA amplitude,  $\xi \equiv X^2 - Y^2$ , contributing to this peak is the excitation of a  $\Lambda$  particle from the  $1s$  to the  $1p$  states with  $\xi = 0.873$ . The total RPA amplitudes for the neutrons and the protons are small ( $\xi = 0.050$  for the neutrons and  $\xi = 0.071$  for the protons), and these values become entirely zero when the  $\Lambda N$  interaction is switched off. The right panel of Fig. 5 shows the transition density for this low-lying dipole state. The neutrons and the protons oscillate in phase, while they move out of phase with the  $\Lambda$  particles. We can thus interpret this mode as a dipole oscillation of the  $\Lambda$  particles against the core nucleus  $^{16}\text{O}$ . This is similar to the soft dipole motion in halo nuclei [36], in which weakly bound valence neutrons oscillate against the core nucleus. We can therefore call the low-lying dipole peak in  $^{18}_{\Lambda\Lambda}\text{O}$  the soft dipole  $\Lambda$  mode. One big difference from the soft dipole mode of halo nuclei is that the  $\Lambda$  particles are located in the center of the hypernucleus whereas the valence neutrons are mainly located in the surface region in halo nuclei due to the Pauli principle. It would be an interesting future work to investigate in more details similarities and differences between the soft dipole mode of halo nuclei and that of hypernuclei.

## 5. Summary

We have discussed the collective excitations of hypernuclei using self-consistent mean-field based theories. We have first investigated the quadrupole deformation of  $\Lambda$  hypernuclei using the relativistic mean field (RMF) theory. We have shown that the deformation disappears for  $^{28}\text{Si}$  when a  $\Lambda$  particle is added. For many other nuclei, the deformation becomes slightly smaller, although the change is not large. We have demonstrated that the dominant effect of the  $\Lambda$  particle on nuclei in the  $sd$ -shell region is to make the deformation smaller, rather than shrinking the size of the whole nucleus. This leads to a reduction of electromagnetic transition probabilities, as we have shown for the  $^{25}_{\Lambda}\text{Mg}$  nucleus using the five dimensional collective Bohr Hamiltonian approach. We have also investigated the vibrational excitations of spherical hypernuclei using the random phase approximation (RPA). We have shown that a new low-lying dipole mode appears in hypernuclei, which can be interpreted as a dipole oscillation of  $\Lambda$  particles against the core nucleus. This is a similar mode as the soft dipole motion in halo nuclei, and thus we call it a soft dipole  $\Lambda$  mode.

For both the collective Hamiltonian and RPA approaches, it is significantly complicated to apply them to single- $\Lambda$  hypernuclei. This involves odd-mass systems with half-integer spins and broken time reversal symmetry. In this article, we have avoided this difficulty by investigating only the core part of single-hypernuclei or by applying the theory to double-hypernuclei. It will be a theoretical challenge to develop a theory for collective excitations of single- $\Lambda$  hypernuclei. Such development will be important in view of research projects currently planned at the J-PARC facility using the new Ge detector array, Hyperball-J, that aims at obtaining new data on the low-lying energy level schemes of  $\Lambda$  hypernuclei in the  $sd$  shell region.

## Acknowledgments

We thank H. Tamura, T. Koike, H. Sagawa, and H.-J. Schulze for useful discussions. This work was supported by the Japanese Ministry of Education, Culture, Sports, Science and Technology by Grant-in-Aid for Scientific Research under the program number (C) 22540262, the National Natural Science Foundation of China under Grants No. 11105111, No. 10947013, and No. 11105110, and the Fundamental Research Funds for the Central Universities (XDKJ2010B007 and XDKJ2010B007).

## References

- [1] T. Motoba, H. Bandō and K. Ikeda, Prog. Theor. Phys. 80 (1983) 189.
- [2] K. Hagino and T. Koike, Phys. Rev. C 84 (2011) 064325.
- [3] E. Hiyama, M. Kamimura, Y. Yamamoto, T. Motoba, and T.A. Rijken, Prog. Theo. Phys. Suppl. 185 (2010) 106.
- [4] J. Žofka, Czech. J. Phys. B30 (1980) 95.
- [5] X.R. Zhou, H.-J. Schulze, H. Sagawa, C.X. Wu, and E.G. Zhao, Phys. Rev. C 76 (2007) 034312.
- [6] M.T. Win and K. Hagino, Phys. Rev. C 78 (2008) 054311.

- [7] H.-J. Schulze, M. Thi Win, K. Hagino and H. Sagawa, Prog. Theo. Phys. 123 (2010) 569.
- [8] M.T. Win, K. Hagino, and T. Koike, Phys. Rev. C 83 (2011) 014301.
- [9] J.M. Yao, Z.P. Li, K. Hagino, M.T. Win, Y. Zhang, and J. Meng, Nucl. Phys. A868-869 (2011) 12.
- [10] B.-N. Lu, E.-G. Zhao, and S.-G. Zhou, Phys. Rev. C 84 (2011) 014328.
- [11] M. Isaka, M. Kimura, A. Dote, and A. Ohnishi, Phys. Rev. C 83 (2011) 044323.
- [12] D. Vretenar, W. Pöschl, G.A. Lalazissis, and P. Ring, Phys. Rev. C 57 (1998) R1060.
- [13] X.-R. Zhou, A. Polls, H.-J. Schulze, and I. Vidaña, Phys. Rev. C 78 (2008) 054306.
- [14] F. Minato, S. Chiba, and K. Hagino, Nucl. Phys. A831 (2009) 150; F. Minato and S. Chiba, Nucl. Phys. A856 (2011) 55 (2011).
- [15] M. Bender, P.H. Heenen, and P.-G. Reinhard, Rev. Mod. Phys. 75 (2003) 121.
- [16] M. Rufa, J. Schaffner, J. Maruhn, H. Stöcker, W. Greiner, and P.-G. Reinhard, Phys. Rev. C 42 (1990) 2469.
- [17] Y. Tanimura and K. Hagino, Phys. Rev. C 85 (2012) 014306.
- [18] G.A. Lalazissis, D. Vretenar, and P. Ring, Phys. Rev. C 55 (1997) 540.
- [19] M. Bender and P.-H. Heenen, Phys. Rev. C 78 (2008) 024309.
- [20] J.M. Yao, J. Meng, P. Ring, and D. Pena Arteaga, Phys. Rev. C 79 (2009) 044312.
- [21] J.M. Yao, J. Meng, P. Ring, and D. Vretenar, Phys. Rev. C 81 (2010) 044311.
- [22] T.R. Rodriguez and J.E. Egido, Phys. Rev. C 81 (2010) 064323.
- [23] T. Niksic, Z.P. Li, D. Vretenar, L. Prochniak, J. Meng, and P. Ring, Phys. Rev. C 79 (2009) 034303.
- [24] Z.P. Li, T. Niksic, D. Vretenar, J. Meng, G.A. Lalazissis, and P. Ring, Phys. Rev. C 79 (2009) 054301.
- [25] A. Bohr and B.R. Mottelson, *Nuclear Structure* (Benjamin, Reading, MA, 1975), Vol. II.
- [26] P. Ring and P. Schuck, *The Nuclear Many Body Problem* (Springer-Verlag, New York, 1980).
- [27] N. Van Giai and H. Sagawa, Phys. Lett. B 106 (1981) 379.
- [28] Y. Yamamoto, H. Bandō, and J. Žofka, Prog. Theo. Phys. 80 (1988) 757.
- [29] P.M. Endt, Nucl. Phys. A510 (1990) 1.
- [30] M. Isaka, H. Homma, M. Kimura, A. Dote, and A. Ohnishi, Phys. Rev. C 85 (2012) 034303.
- [31] G.F. Bertsch and R.A. Broglia, *Oscillations in Finite Quantum Systems* (Cambridge University Press, Cambridge, 1994).
- [32] K. Yoshida and T. Nakatsukasa, Phys. Rev. C 83 (2011) 021304(R).
- [33] F. Minato and K. Hagino, Phys. Rev. C 85 (2012) 024316.
- [34] J. Bartel, P. Quentin, M. Brack, C. Guet, and H.B. Hakansson, Nucl. Phys. A386 (1982) 79.
- [35] D.E. Lansky, Phys. Rev. C 58 (1988) 3351.
- [36] K. Ikeda, T. Myo, K. Kato, and H. Toki, Lecture Notes in Physics 818 (2010) 165.